New Phytologist

ETHYLENE RESPONSE FACTOR 115 integrates jasmonate and cytokinin signaling machineries to repress adventitious rooting in Arabidopsis

Abdellah Lakehal[1] (iD), Asma Dob[1] (iD), Zahra Rahneshan[1,2] (iD), Ondřej Novák[3,4] (iD), Sacha Escamez[1] (iD), Sanaria Alallaq[1] (iD), Miroslav Strnad[3] (iD), Hannele Tuominen[1] (iD) and Catherine Bellini[1,5] (iD)

[1]Department of Plant Physiology, Umeå Plant Science Center, Umeå University, SE-90736 Umeå, Sweden; [2]Department of Biology, Faculty of Science, Shahid Bahonar University, Kerman 76169-14111, Iran; [3]Laboratory of Growth Regulators, Faculty of Science, Palacký University and Institute of Experimental Botany, The Czech Academy of Sciences, 78371 Olomouc, Czech Republic; [4]Department of Forest Genetics and Physiology, Umeå Plant Science Center, Swedish Agriculture University, SE-90183 Umea, Sweden; [5]Institut Jean-Pierre Bourgin, INRAE, AgroParisTech, Université Paris-Saclay, FR-78000 Versailles, France

Summary

• Adventitious root initiation (ARI) is a de novo organogenesis program and a key adaptive trait in plants. Several hormones regulate ARI but the underlying genetic architecture that integrates the hormonal crosstalk governing this process remains largely elusive.
• In this study, we use genetics, genome editing, transcriptomics, hormone profiling and cell biological approaches to demonstrate a crucial role played by the APETALA2/ETHYLENE RESPONSE FACTOR 115 transcription factor.
• We demonstrate that ERF115 functions as a repressor of ARI by activating the cytokinin (CK) signaling machinery. We also demonstrate that ERF115 is transcriptionally activated by jasmonate (JA), an oxylipin-derived phytohormone, which represses ARI in NINJA-dependent and independent manners. Our data indicate that NINJA-dependent JA signaling in pericycle cells blocks early events of ARI.
• Altogether, our results reveal a previously unreported molecular network involving cooperative crosstalk between JA and CK machineries that represses ARI.

Introduction

Adventitious rooting is a post-embryonic developmental program and key adaptive trait in plants. Plants develop adventitious roots (ARs) in response to diverse intrinsic and/or extrinsic (stress-induced) cues such as wounding, darkness, flooding, nutrient and water availability (Bellini et al., 2014; Steffens & Rasmussen, 2016). These cues are perceived by competent cells and trigger extensive (epi) genetic reprogramming that results in targeted cells acquiring new identities (Bellini et al., 2014; Lakehal & Bellini, 2018). The process has fundamental interest and practical importance as adventitious rooting is often a limiting step in clonal propagation of many plant species. Clonal propagation is widely used in agricultural practices and forest nurseries to maintain and reproduce elite genotypes. Previous studies showed the importance of phytohormones such as auxin, jasmonate (JA) and cytokinins (CK) in regulating AR initiation (ARI) (Lakehal & Bellini, 2018), but the mechanisms underlying the crosstalk between these phytohormones during ARI remain elusive.

JA, a stress-induced phytohormone, plays crucial roles in plant immunity and defense against herbivorous insects (Wasternack & Hause, 2013). It also participates in control of diverse developmental processes, including tissue regeneration and rhizotaxis (Wasternack & Hause, 2013; Lakehal et al., 2020). The isomer (+)-7-iso-JA-Ile (JA-Ile), the bioactive form of JA (Fonseca et al., 2009), is perceived by the F-box protein CORONATINE INSENSITIVE1 (COI1), which is an integral component of the Skp-Cullin-F-box (SCF) complex (Xie et al., 1998). The COI1 receptor fine-tunes the function of the JA transcriptional machinery in a simple manner. Briefly, in the resting state, marked by low JA-Ile contents, the transcriptional activity of a number of transcription factors, including the basic-Helix-loop-Helix MYC, is repressed by JASMONATE ZIM DOMAIN (JAZ) repressors through either physical interaction or recruitment of the general co-repressor TOPLESS (TPL) or TPL-related proteins (TPRs) (Chini et al., 2007; Thines et al., 2007; Yan et al., 2007). The adaptor NOVEL INTERACTOR OF JAZ (NINJA) mediates interaction of JAZs with TPL or TRPs (Pauwels et al., 2010). During activation, marked by accumulation of JA-Ile, JAZs form co-receptor complexes with COI1. This interaction is facilitated by JA-Ile, which acts as a molecular glue (Sheard et al., 2010). Formation of the co-receptor complexes triggers ubiquitylation and proteasome-dependent degradation of the targeted JAZs, thereby releasing the transcription factors to transcriptionally

induce or repress their downstream target genes. Biochemical studies suggest that JAZ-dependent repression machinery can inhibit the transcriptional activity of different MYCs in different ways, depending on the JAZ protein involved (Chini *et al.*, 2016). However, the biological roles of this multilayered regulation are unclear, largely because multiple *jaz* mutations may cause phenotypic deviations, but not single loss-of-function mutations (Campos *et al.*, 2016; Guo *et al.*, 2018).

JA signaling counteracts or cooperates with a number of hormonal and signaling cascades in the control of plant growth and development (Wasternack & Hause, 2013). We have previously shown that the COI1-dependent MYC2-mediated JA signaling inhibited the intact hypocotyl-derived ARI downstream of the auxin signaling machinery (Gutierrez *et al.*, 2012) (Fig. 1). Accordingly, in contrast to the *MYC2*-overexpressing line *35S: MYC2*, the loss-of-function mutant *myc2* produces more ARs than wild-type plants, indicating that MYC2 plays an important role in inhibition of ARI downstream of auxin (Gutierrez *et al.*, 2012). Recently, we also showed that the TIR1- and AFB2-dependent auxin signaling pathways promote ARI by negatively controlling JA content (Lakehal *et al.*, 2019a). However, despite evidence of its central role in modulating ARI, the basis (genetic and mechanistic) and downstream targets of the MYC2-mediated JA signaling involved in this process remained unclear.

Recently, Zhou and collaborators (Zhou *et al.*, 2019) showed that two members of subgroup X of the *APETALA2/ETHYLENE RESPONSE FACTOR (ERF)* family (*ERF109 and ERF115*) promote root stem cell niche replenishment and tissue regeneration after excision, and their expression is directly controlled by MYC2-mediated JA signaling. The *ERF115* transcription factor

and its two closest homologs, *ERF114* (also known as *ERF BUD ENHANCER (EBE)*) and *ERF113* (also known as *RELATED to AP2.6L, RAP2.6L*) have been shown to control various regenerative processes, such as callus formation, tissue repair, root stem cell niche maintenance and root growth (Che *et al.*, 2006; Nakano *et al.*, 2006; Asahina *et al.*, 2011; Mehrnia *et al.*, 2013; Heyman *et al.*, 2016; Ikeuchi *et al.*, 2018; Kong *et al.*, 2018; Yang *et al.*, 2018). The three genes are rapidly induced by mechanical wounding (Ikeuchi *et al.*, 2017), suggesting that they play an important role in connecting the stress-induced JA signaling machinery with other signaling cascades in provision of correct cell-fate and/or developmental inputs for organogenesis processes. However, how these genes coordinate and integrate the stress-induced hormonal pathways to ensure these multifunctionalities is still largely unclear. Here we provide evidence that the JA signaling machinery inhibits ARI in both NINJA-dependent and NINJA-independent manners, and the JA-induced *ERF115* transcription factor inhibits this process in a CK-dependent manner, suggesting that CKs act downstream of JA in ARI inhibition.

Materials and Methods

Plant material

The quadruple mutant *jaz7jaz8jaz10jaz1 3* (Thireault *et al.*, 2015) and quintuple mutant *jaz1jaz3jaz4jaz9jaz10* (Campos *et al.*, 2016) were provided by G. Howe (Michigan State University, East Lansing, MI, USA). The single mutants *ninja-1*, *ninja-2* (Acosta *et al.*, 2013), and *myc2-322B* as well as the double mutants *ninja-1myc2-322B*, *ninja-2myc2-322B* and *ninja-1atr2D* (Gasperini *et al.*, 2015) were provided by E.E. Farmer (University of Lausanne, Switzerland). The gain of function allele of *MYC3* (*atr2D*) (Smolen *et al.*, 2002) was provided by J. Bender (Brown University, Providence, RI, USA). The single mutant *erf115* (SALK_021981) and transgenic lines *pERF115:ERF115: SRDX*, and *35S:ERF115* (Heyman *et al.*, 2013) were provided by L. De Veylder (VIB, University of Gent, Belgium). The *rap2-6l-1* mutant (SALK_051006) (Che *et al.*, 2006), *arr1-3arr11-2* (N6980) and *arr1-3arr11-2 arr12-1* (N6986) were provided by the Nottingham Arabidopsis Stock Centre (UK). The transgenic line *35S:CKX1* (Werner *et al.*, 2003) and triple mutant *ipt3ipt5ipt7* (Miyawaki *et al.*, 2006) were provided by T. Schmülling (Freie Universität, Berlin, Germany). E. E. Farmer and L. De Veylder also respectively provided the reporter lines *pMYC2:GUSplus*, *pNINJA:GUSplus* and *pNINJA:NINJA: mCITRINE/ninja-1* (Gasperini *et al.*, 2015) and *pERF115:GUS* (Heyman *et al.*, 2013).

CRISPR-Cas9 cloning, transformation and mutant screening

To generate the loss-of-function allele *erf114*C, two guide RNAs (ERF114_F and ERF114_R, see later Supporting Information Table S2) were designed, as previously described (Lakehal *et al.*, 2019b), to target the *ERF114* gene's first exon (Fig. S3, see later). The guide RNAs were then cloned into the binary vector
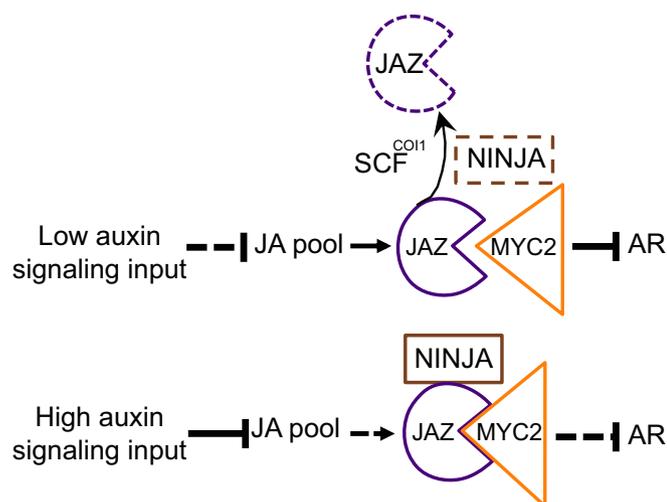

Fig. 1 A genetic model for the action of jasmonate (JA) signaling components during adventitious root initiation (ARI) in Arabidopsis. With a low auxin signaling input, the JA pool increases in the hypocotyl. This triggers degradation of the targeted JAZs, thereby releasing transcriptional activity of the MYC2, MYC3, MYC4 and inhibiting ARI. With a high auxin signaling input, the JA pool decreases in the hypocotyl, thereby repressing the MYC-mediated JA signaling machinery and increasing ARI (Gutierrez *et al.*, 2012; Lakehal *et al.*, 2019a).

pHEE401E, the resulting construct was transformed into *Escherichia coli* cells, and the positive clones were selected by PCR, then confirmed by sequencing, following previous protocols (Xing *et al.*, 2014; Wang *et al.*, 2015). The *Agrobacterium*-mediated floral dip method (Clough & Bent, 1998) was used to transform the construct into *rap2-6l-1* or *erf115* mutants. T1 seedlings were screened on Arabidopsis growth medium (Lakehal *et al.*, 2019b) containing 50 µg ml^{-1} hygromycin and surviving seedlings were genotyped for deletions in *ERF114* using primers listed in Table S2 (see later). Several independent homozygous and heterozygous T1 lines were identified. Only homozygous *erf114C* and Cas9-free lines, confirmed by examination of T2 individuals and Cas9-construct genotyping (Xing *et al.*, 2014; Wang *et al.*, 2015), were used for further analysis.

Tissue-specific complementation: cloning, transformation and transgenic line screening

The pEN-L4-pGATA23-R1 and pEN-L4-pXPP-R1 plasmids (De Rybel *et al.*, 2010; Andersen *et al.*, 2018) were gifts from T. Beeckman (VIB, Gent, Belgium) and J. Vermeer (University of Zurich, Switzerland), respectively. Plasmids carrying coding sequences of the *NINJA* gene, pEN-L1-NINJA(noSTOP)-L2, and reporter protein, pEN-R2-mCITRINE-L3 (Gasperini *et al.*, 2015), were gifts from E.E. Framer (University of Lausanne, Switzerland). To generate promoter:NINJA:CT fusion protein constructs, the pEN-L4-promoter-R1, pEN-L1-NINJA (noSTOP)-L2 and pEN-R2-mCITRINE-L3 were recombined into the pB7m34gw vector using LR clonaseII plus (Invitrogen, Carlsbad, CA, USA) according to the manufacturer's instructions. All the expression vectors were confirmed by colony PCR and sequencing, then transformed into GV3101 *Agrobacterium tumefaciens* cells, which were used to transform *ninja-1myc2-332B* double mutants using the floral dip method (Clough & Bent, 1998). Single-copy, homozygous lines were selected by cultivating representatives of T2 and T3 generations on Arabidopsis medium (Lakehal *et al.*, 2019b) supplemented with 10 µg ml^{-1} DL-phosphinothricin (Duchefa Biochemie, Haarlem, the Netherlands, https://www.duchefa-biochemie.com/). At least two lines carrying each construct showing the same phenotype were further characterized.

Growth conditions and root (adventitious and lateral) phenotyping

Previously described adventitious rooting conditions (Sorin *et al.*, 2005; Gutierrez *et al.*, 2009, 2012; Lakehal *et al.*, 2019a) were applied in all the experiments. Seedlings were etiolated in the dark until the hypocotyls were approximatively 6–7 mm long, then were grown in long-day conditions (22°C : 17°C, 16 h : 8 h, light : dark cycles, with 130–140 µmol photons m^{-2} s^{-1} during light phases and constant 65% relative humidity). After 7 days, numbers of primordia and emerged ARs were counted under a binocular stereomicroscope. Numbers of visible lateral roots (LRs) were also counted, and the primary root length was measured using IMAGEJ software (Schindelin *et al.*, 2012). The LR density was calculated by dividing the number of LR by the primary root length.

RNA isolation and cDNA synthesis

Total RNA was prepared using a RNAqueous® Total RNA Isolation kit (Ambion™, Austin, TX, USA). Portions (4 µg) of the resulting RNA preparations were treated with DNaseI using a DNA*free* Kit (Ambion) then cDNA was synthesized by reverse transcription using a SuperScript II Reverse transcriptase kit (Invitrogen) with anchored-oligo(dT)$_{18}$ primers, according to the manufacturer's instructions.

Quantitative RT-PCR experiments

Transcript levels were assessed by real-time quantitative reverse transcription polymerase chain reaction (qRT-PCR), in assays with triplicate reaction mixtures (final volume, 20 µl) containing 5 µl of cDNA, 0.5 µM of both forward and reverse primers, and 1 × LightCycler 480 SYBR Green I Master (Roche, Basel, Switzerland) using a LightCycler 480 instrument (Roche) according to the manufacturer's instructions. A melting curve analytical step was added to each PCR program. The sequences of primers used for all target genes are presented in Table S1. The crossing threshold (CT) values for each sample were acquired with the LightCycler 480 software (Roche) using the second derivative maximum method. All quantifications were repeated with at least two independent biological replicates.

Quantitative RT-PCR data analysis

Reference genes were validated as the most stably expressed genes in our experimental procedures (Gutierrez *et al.*, 2009) using GenNorm software and the most stable two (*TIP41* and *EF1A*) were used to normalize the quantitative PCR data. The data obtained using both reference genes were similar and only data obtained using *TIP41* are presented here. Relative transcript amounts were calculated as previously described (Gutierrez *et al.*, 2009), and considered significant if fold differences were ≥ 1.5 with *P*-values ≤ 0.05).

RNA sequencing and transcriptomic analysis

Total RNA was extracted from etiolated hypocotyls grown in darkness at T0, just before exposure of some of the etiolated seedlings to light. Further samples were collected after 9 and 24 h in long-day conditions (T9L and T24L, respectively). In each case three biological replicates were prepared, and the total RNA was treated with DNaseI using a DNA*free* Kit (Ambion™) to remove any contaminating DNA. The RNA's integrity and quantity were checked using a 2100 Bioanalyzer (Agilent, Santa Clara, CA, USA), then it was sequenced by BGI Tech (Shenzhen, China) using an Illumina HiSeq 4000 platform. The reads were trimmed with SOAPnuke then clean reads were mapped to the Araport11 reference sequence using Bowtie2 (Langmead & Salzberg, 2012). Gene expression was quantified using RSEM

(RNA-Seq by Expectation-Maximization) (Li & Dewey, 2014) and differentially expressed genes (DEGs) between *ninja-1myc2-322B* and wild-type plants at selected time points were detected using NOISEQ software (Tarazona *et al.*, 2011) with fold change ≥ 2 and probability 0.8 settings.

FIMO tools were used, via the http://meme-suite.org/tools/fimo web interface, to scan promoters (1 Kb upstream of ATG translation start codons) of the DEGs for G box and G-box-like motifs with a 1E-4 *P*-value setting.

RNA-seq data has been deposited at the European Nucleotide Archive (ENA) – https://www.ebi.ac.uk/ena and will be available using the following accession number PRJEB36195.

Spatiotemporal gene expression patterns during ARI

The spatiotemporal patterns of *NINJA*, *MYC2* and *ERF115* genes' expression during ARI were monitored by GUS-based analysis, as follows. Seedlings expressing *pNINJA:GUSplus*, *pMYC2:GUSplus* or *pERF115:GUS* were grown in AR-inducing conditions as described earlier, then stained with X-GLCA (X1405.1000; Duchefa Biochemie) as previously described (Sorin *et al.*, 2005). At least 25 seedlings of each genotype sampled at each time point were stained, and one representative seedling of each set was photographed.

Sample preparation for hormone quantification

Hypocotyls were collected from seedlings grown in AR-inducing conditions as described earlier. The hypocotyls were quickly dried on tissue paper then frozen in liquid nitrogen. Samples were prepared from six biological replicates.

Quantification of *cis*-OPDA, JA and JA-Ile

Endogenous levels of jasmonates (*cis*-OPDA, free JA and JA-Ile) were determined in 20 mg samples, as previously described (Floková *et al.*, 2014).

Quantification of endogenous CK bases

Cytokinin metabolites were quantified following published methodology (Svačinová *et al.*, 2012; Antoniadi *et al.*, 2015). Briefly, samples (20 mg fresh weight (FW)) were homogenized and extracted in 1 ml of modified Bieleski solvent (60% methanol (MeOH), 10% methanoic acid (HCOOH) and 30% water (H_2O)) together with a cocktail of stable isotope-labeled internal standards (0.25 pmol of CK bases, ribosides, *N*-glucosides, and 0.5 pmol of nucleotides added per sample). The extracts were applied to an Oasis MCX column (30 mg ml^{-1}, Waters, Milford, MA, USA) conditioned with 1 ml each of 100-% MeOH and H_2O, equilibrated sequentially with 1 ml of 50% (v/v) nitric acid, 1 ml of H_2O, and 1 ml of 1 M HCOOH, then washed with 1 ml of 1 M HCOOH and 1 ml 100% MeOH. Analytes were then eluted in two steps with 1 ml of 0.35 M aqueous ammonium hydroxide (NH_4OH) solution and 2 ml of 0.35 M NH_4OH in 60% (v/v) MeOH solution, evaporated to dryness *in vacuo* and stored at −20°C. Cytokinin levels were determined by ultra-high performance liquid chromatography-electrospray tandem mass spectrometry (UHPLC-MS/MS) using stable isotope-labeled internal standards as reference compounds (Rittenberg & Foster, 1940). Following separation with an Acquity UPLC® system (Waters) equipped with an Acquity UPLC BEH Shield RP18 column (150 mm × 2.1 mm dimensions, 1.7 µm particles; Waters), the effluent was introduced into the electrospray ion source of a Xevo™ TQ-S MS triple quadrupole mass spectrometer (Waters). Six independent biological replicates of each genotype sampled at each time point were analyzed.

Confocal laser scanning microscopy (CLSM) analysis

Images of the vasculature in *Arabidopsis* hypocotyls at depths up to 150 µm from the epidermal surface were acquired using a Zeiss LSM880 inverted confocal laser scanning microscope (Carl Zeiss GmbH, Oberkochen, Germany) equipped with a C-Achroplan 32×/0.85 W Corr M27 lens. The seedlings were etiolated in the dark until their hypocotyls were 6–7 mm long then incubated in liquid medium containing 30 µg ml^{-1} propidium iodide (PI) as a cell wall counter-stain to identify the cell layers, and observed while still alive, mounted with the same medium. The PI was excited using a 561 nm laser while expressed reporter protein (mCITRINE) was excited with a 488 nm Argon laser, using a MBS 488/561 Main Beam Splitter. PI fluorescence from PI and the reporter (mCITRINE) were detected to localize expression with a photomultiplier tube (PMT) detector and a GaAsP (gallium arsenide phosphide photomultiplier tube) 32-channels spectral detector (with about two times higher sensitivity than the PMT, enabling detection of even poorly expressed reporters), respectively. Three-dimensional (3D) projections and orthogonal views were generated using FIJI/IMAGEJ (Schindelin *et al.*, 2012), including image-wide adjustments of brightness and contrast for each channel before merging to ensure that both signals from PI and the fluorescent protein reporter could be easily seen in all displayed images.

Results

NINJA-dependent and NINJA-independent JA signaling repress ARI

To better understand the role of JA signaling during intact hypocotyl-derived ARI (Fig. 1), we first analyzed the AR phenotype of multiple *jaz* mutants, under previously described conditions (Sorin *et al.*, 2005; Gutierrez *et al.*, 2009, 2012). The quadruple loss-of-function mutant *jaz7jaz8jaz10jaz13* (Thireault *et al.*, 2015) had the same phenotype as the wild type, whereas the quintuple mutant *jazQ* (*jaz1jaz3jaz4jaz9jaz10*) (Campos *et al.*, 2016) produced slightly fewer ARs than wild-type plants (Fig. 2a). These data confirm the high functional redundancy of the 13 *JAZ* genes in the Arabidopsis genome (Chini *et al.*, 2007, 2016; Thines *et al.*, 2007; Yan *et al.*, 2007; Thireault *et al.*, 2015), which complicates characterization of their specificity.
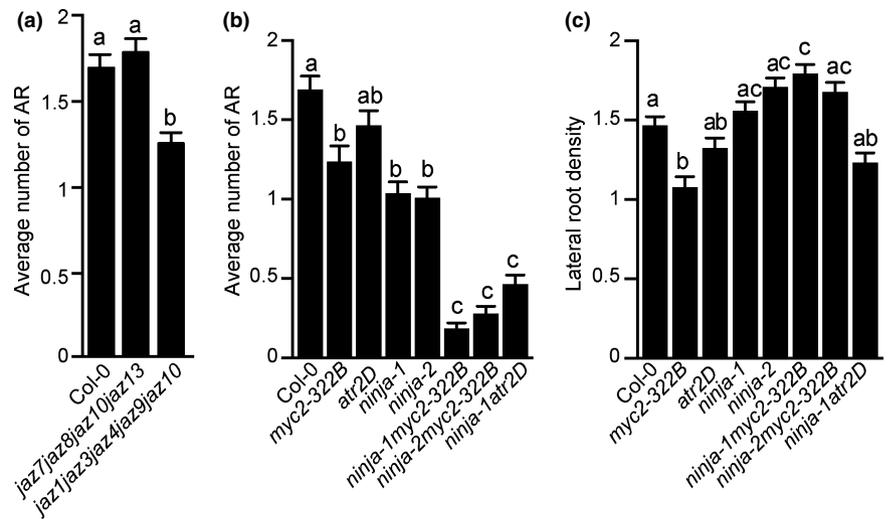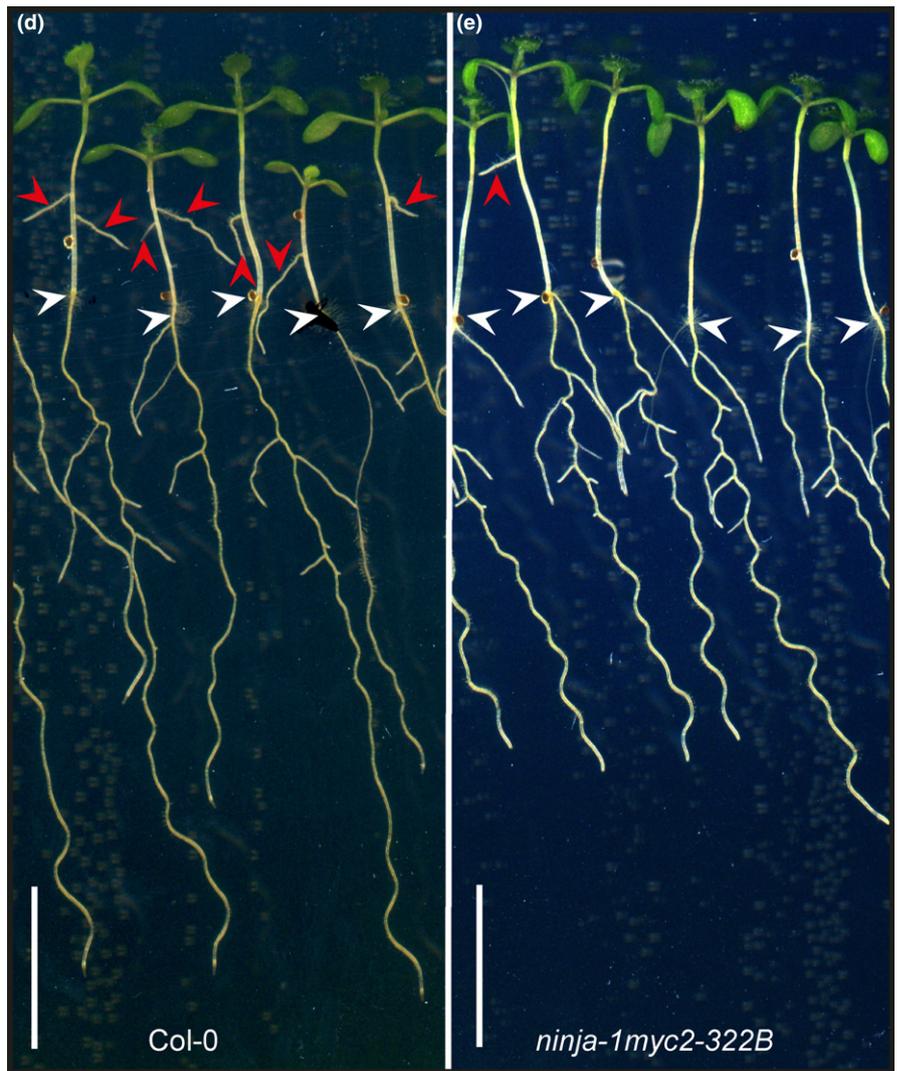
Fig. 2 Jasmonate (JA) signaling inhibits adventitious root initiation in Arabidopsis in NINJA-dependent and NINJA-independent manners. (a) Average number of adventitious roots (ARs) observed in indicated multiple *jaz* mutants and wild-type (Col-0) seedlings. Data from three independent biological replicates, each of at least 40 seedlings, were pooled and averaged. One-way analysis of variance (ANOVA) combined with Tukey's multiple comparison post-tests showed that the *jaz1jaz3jaz4jaz9jaz10* quintuple mutant produced significantly less ARs than wild-type plants (denoted by letters). Error bars indicate ± SEM ($n \geq 40$; $P < 0.05$). (b) Average number of ARs produced by JA signaling mutants. Data from two independent biological replicates, each of at least 40 seedlings, were pooled and averaged. A nonparametric Kruskal–Wallis test followed by Dunn's multiple comparison test indicated significant differences in AR number (denoted by letters). Error bars indicate ± SEM ($n \geq 40$; $P < 0.02$). (c) Lateral root density of JA signaling mutants and wild-type seedlings grown in AR phenotyping conditions. One-way ANOVA combined with Tukey's multiple comparison post-test indicated that the *myc2-322B* and *ninja-1myc2-322B* mutants had slightly lower and slightly higher than wild-type lateral root (LR) densities, respectively (denoted by letters). Error bars indicate ± SEM ($n \geq 40$; $P < 0.05$). (d, e) Representative photographs of (d) wild-type and (e) *ninja-1myc2-322B* double mutant seedlings. Bars, 6 mm. Arrowheads indicate hypocotyl-root junctions (white) or ARs (red).

Therefore, we analyzed the phenotype of the gain-of-function mutant *myc2-322B*, which harbors a point mutation in the transcriptional activation domain (TAD) that changes glutamate 165 to lysine. This prevents MYC2's interaction with most JAZ repressor proteins, resulting in almost constitutive MYC2 signaling (Gasperini *et al.*, 2015). We found that *myc2-322B* produced slightly fewer AR than wild-type plants (Fig. 2b), in accordance with our previous findings that the loss-of-function mutant *myc2*

and overexpressing line *35S:MYC2* respectively produced more and less ARs than wild-type counterparts (Gutierrez *et al.*, 2012). We also analyzed the AR phenotype associated with two loss-of-function *ninja* (*ninja-1* and *ninja-2*) alleles (Acosta *et al.*, 2013), because the NINJA adaptor is a central hub in the transcriptional repression machinery that inactivates MYC transcription factors (Pauwels *et al.*, 2010) (Fig. 1). The *ninja-1* and *ninja-2* mutants produced significantly fewer ARs than wild-type plants (Fig. 2b), but their phenotypic deviation is weak, presumably due to presence of a NINJA-independent pathway that continues to repress MYCs and thus allows ARI. Because MYC2 acts additively with MYC3 and MYC4 in the inhibition of ARI (Gutierrez *et al.*, 2012), we hypothesized that removing NINJA in a *myc2-322B* background might abolish the remaining NINJA-dependent repression and hence release activity of the three MYCs. De-repression of these transcription factors would then result in constitutively enhanced MYC-mediated JA signaling and block the ARI process. To test this hypothesis, we analyzed the AR phenotype of two independent double mutants: *ninja-1myc2-322B* and *ninja-2myc2-322B* (Gasperini *et al.*, 2015). We found that ARI was almost completely inhibited in both double mutants, confirming the inhibitory effect of JA (Fig. 2b–e). As expected, the double mutants had shorter primary roots (PRs) than wild-type plants, due to the inhibitory effect of JA signaling on PR growth (Staswick *et al.*, 1992) and fewer LRs (Fig. S1a,b), but the LR density was not affected (Fig. 2c). To get further genetic evidence, we also analyzed the AR phenotype of the gain-of-function mutant *atr2D*, which harbors a point mutation in the JAZ interaction domain (JID) of the MYC3 protein (Smolen *et al.*, 2002) that prevents its interaction with a subset of JAZ repressors (Zhang *et al.*, 2015). Notably, there was no significant difference in AR numbers of *atr2D* mutants and wild-type plants, but the *ninja-1atr2D* double mutant produced far fewer ARs (Fig. 2b), confirming the *atr2D* mutation's additive effect and the role of MYC3 in the control of AR formation. Collectively, these results genetically confirm the importance of the NINJA-dependent and NINJA-independent pathways in the control of ARI.

NINJA and *MYC2* are expressed in the etiolated hypocotyl

To examine spatiotemporal expression patterns of the *NINJA* and *MYC2* genes during early ARI events, we used seedlings harboring *pNINJA:GUS* or *pMYC2:GUS* transcriptional fusions (Gasperini *et al.*, 2015). The seedlings were grown in ARI-inducing conditions in the dark and sampled for *pNINJA:GUS* or *pMYC2:GUS* expression analysis at T0, just before some of the etiolated seedlings were exposed to light. Further samples were collected at T9L and T24L (after 9 and 24 h growth in long-day conditions, respectively), while controls were sampled at T9D and T24D (after a further 9 and 24 h growth in the dark, respectively). The two promoters were shown to be constitutively active in all the organs at all time points, although *MYC2* promoter activity declined in the cotyledons over time (Fig. 3a–e). These data indicate that *NINJA* and *MYC2* genes have overlapping expression domains in the hypocotyl.

Expressing NINJA in xylem-pole pericycle cells is sufficient to counter JA's negative effect during ARI

We confirmed that the NINJA protein was broadly expressed in the hypocotyl, including the xylem-pole pericycle (xpp) cells (Fig. 3f) where ARs are initiated (Sorin *et al.*, 2005; Sukumar *et al.*, 2013). We then assessed whether re-activating the NINJA-dependent JA repression machinery in those cells would be sufficient to restore ARI in the *ninja1-myc2-322B* double mutant. For this, we produced translational fusions of NINJA with the mCITRINE reporter driven by two xpp cell-specific promoters, *GATA23* (De Rybel *et al.*, 2010) and *XPP* (Andersen *et al.*, 2018). The p*GATA23:NINJA:mCITRINE* or p*XPP:NINJA:mCITRINE* constructs were introduced into the *ninja-1myc2-322B* double mutant, and we confirmed that the NINJA:mCITRINE protein was specifically present in the hypocotyl xpp cells (Fig. 3g, h). We analyzed the AR phenotype of two independent lines carrying each construct and showed that in both cases the effect of the *ninja-1* mutation was complemented (Fig. 3i). These results suggest that expressing NINJA in xpp cells is sufficient to de-repress ARI, and that NINJA-dependent JA signaling acts in early stages of ARI.

Transcriptomic insights into JA's role in ARI

To get mechanistic insights into how JA signaling reprograms the transcriptional machinery during ARI, we compared transcriptomes of *ninja-1myc2-322B* double mutant and wild-type hypocotyls at three time points: T0, T9 and T24 (Fig. 4a). In T0 samples we detected 530 DEGs, of which 462 were upregulated and 68 downregulated in the *ninja-1myc2-322B* double mutant. We detected 671 DEGs at T9, 453 upregulated and 218 downregulated, and 579 at T24, 388 upregulated and 191 downregulated (Figs 4b, S2; Table S2).

The *ninja-1myc2-322B* double mutant has a constitutive JA response signature

MYC transcription factors recognize and bind to hexameric *cis*-regulatory G-box motifs (CACGTG or CACATG), and MYC2 binds to G box-like motifs (AACGTG, CATGTG, CACGAG, CACATG, CACGCG) with differing affinities (Godoy *et al.*, 2011). To get an overview of possible direct targets of MYCs among the DEGs, we searched for these motifs in the 1 kb regions upstream of their ATG translation start codons. We found that DEGs' promoters are highly enriched with MYC binding sites, suggesting that they include potential direct targets of MYC. At T0, T9 and T24, 64% of 520 DEGs (342: 334 upregulated and eight downregulated), 62% of 671 DEGs (420: 341 upregulated and 79 downregulated), and 67% of 579 DEGs (389: 287 upregulated and 102 downregulated) respectively contained at least one of the six motifs (Fig. 4c).

Most of the *JAZ* genes, which are early JA-responsive genes, were highly upregulated in the *ninja-1myc2-322B* double mutant at all sampling time points (Fig. 4d), confirming the presence of enhanced, constitutive JA signaling. Accordingly, several genes
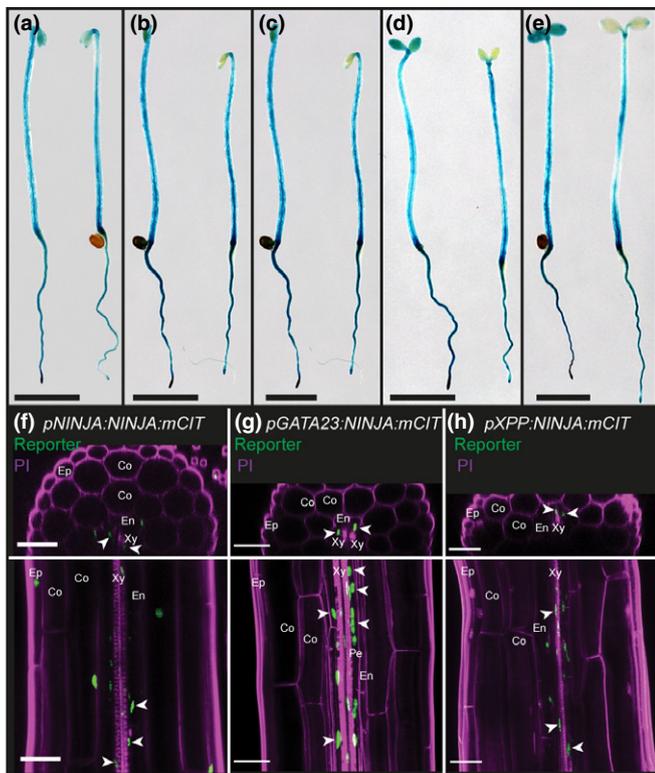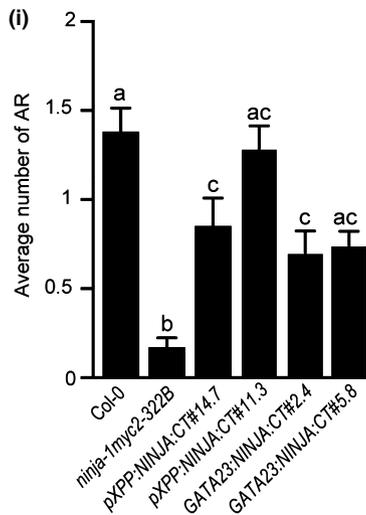
Fig. 3 NINJA-dependent jamonate (JA) signaling inhibits adventitious root initiation (ARI) in pericycle cells of Arabidopsis hypocotyl. (a–e) Spatiotemporal activity patterns of the *NINJA* and *MYC2* promoters, left and right, respectively in each panel. Seedlings expressing the *pNINJA: GUSplus* or *pMYC2:GUSplus* constructs were grown in the dark until their hypocotyls were 6–7 mm long (T0) (a) then either kept in the dark for 9 h (T9D) (b) and 24 h (T24D) (c) or transferred to the light for 9 h (T9L) (d) or 24 h (T24L) (e). Bars, 6 mm. (f–h) Representative images of etiolated hypocotyls expressing *pNINJA:NINJA:mCITRINE* (f), *pGATA23:NINJA: mCITRINE* (g), and *pXPP:NINJA:mCITRINE* (h) of seedlings grown in darkness until their hypocotyls were 6–7 mm long. The cell walls were counterstained magenta with propidium iodide (PI). Orthogonal views from epidermis to vasculature are shown in the upper panels. Z-projections of the hypocotyl volume around the vasculature are shown in the lower panels. The following cell types can be distinguished: epidermis (Ep), cortex (Co), endodermis (En), pericycle (Pe) and xylem (Xy). In orthogonal views, the two protoxylem elements allow deduction of the direction of the xylem axis and thus the position of the xylem-pole pericycle. Arrowheads indicate signals in xylem-pole pericycle cells in green. Bars, 50 μm. (i) Average numbers of adventitious roots (ARs) produced by the *ninja-1myc2-322B* double mutant, two independent transgenic lines expressing *pXPP:NINJA:mCITRINE/ninja-1myc2-322B* or *pGATA23: NINJA:mCITRINE/ninja-1myc2-322B* and wild-type (Col-0) seedlings. A nonparametric Kruskal–Wallis test followed by Dunn's multiple comparison post-test indicated that the wild type, *pXPP:NINJA: mCITRINE/ninja-1myc2-322B* (#14.7 and #11.3) and *pGATA23:NINJA: mCITRINE/ninja-1myc2-322B* (#2.4 and #5.8) produced significantly more ARs than the *ninja1myc2-322B* double mutant (denoted by letters). Error bars indicate ± SEM ($n \geq 30$; $P < 0.006$).

JA signaling controls expression of *ERF113*, *ERF114* and *ERF115* transcription factors

The candidate transcription factor potential targets of MYC2 we detected included three closely related members of subgroup X of the *ERF* family (*ERF113*, *ERF114* and *ERF115*) (Fig. 5a,b). Analysis by qRT-PCR confirmed that these three genes were all upregulated in the hypocotyl of the *ninja-1myc2-322B* double mutant, except *ERF113* at T0 (Fig. 5c). These genes have known involvement in a number of organogenesis and regeneration processes (Heyman *et al.*, 2018). To address their role in ARI, we analyzed the AR phenotypes of available single loss of *ERF113* or *ERF115* function mutants (*rap2.6l-1* and *erf115*, respectively) and observed no significant difference in this respect between them and wild-type controls (Fig. 6a). As no loss-of-function T-DNA line for *ERF114* was available, we used CRISPR-Cas9 technology to delete a *c.* 40 bp genomic fragment in the first exon of the *ERF114* gene in the *rap2.6l-1* and the *erf115* backgrounds to obtain *rap2.6l-1erf114C* and *erf115erf114C* double mutants, respectively (Fig. S3). Other multiple mutants were obtained by genetic crosses. Only the triple mutant *rap2.6l-1erf114Cerf115* produced significantly more ARs than wild-type controls (Fig. 6a), indicating that *ERF113*, *ERF114* and *ERF115* act redundantly in the control of ARI.

ERF115 represses hypocotyl-derived ARI downstream of auxin

Previous findings that *ERF115*'s expression is directly controlled by MYC2 and it plays major roles in root regeneration and stem
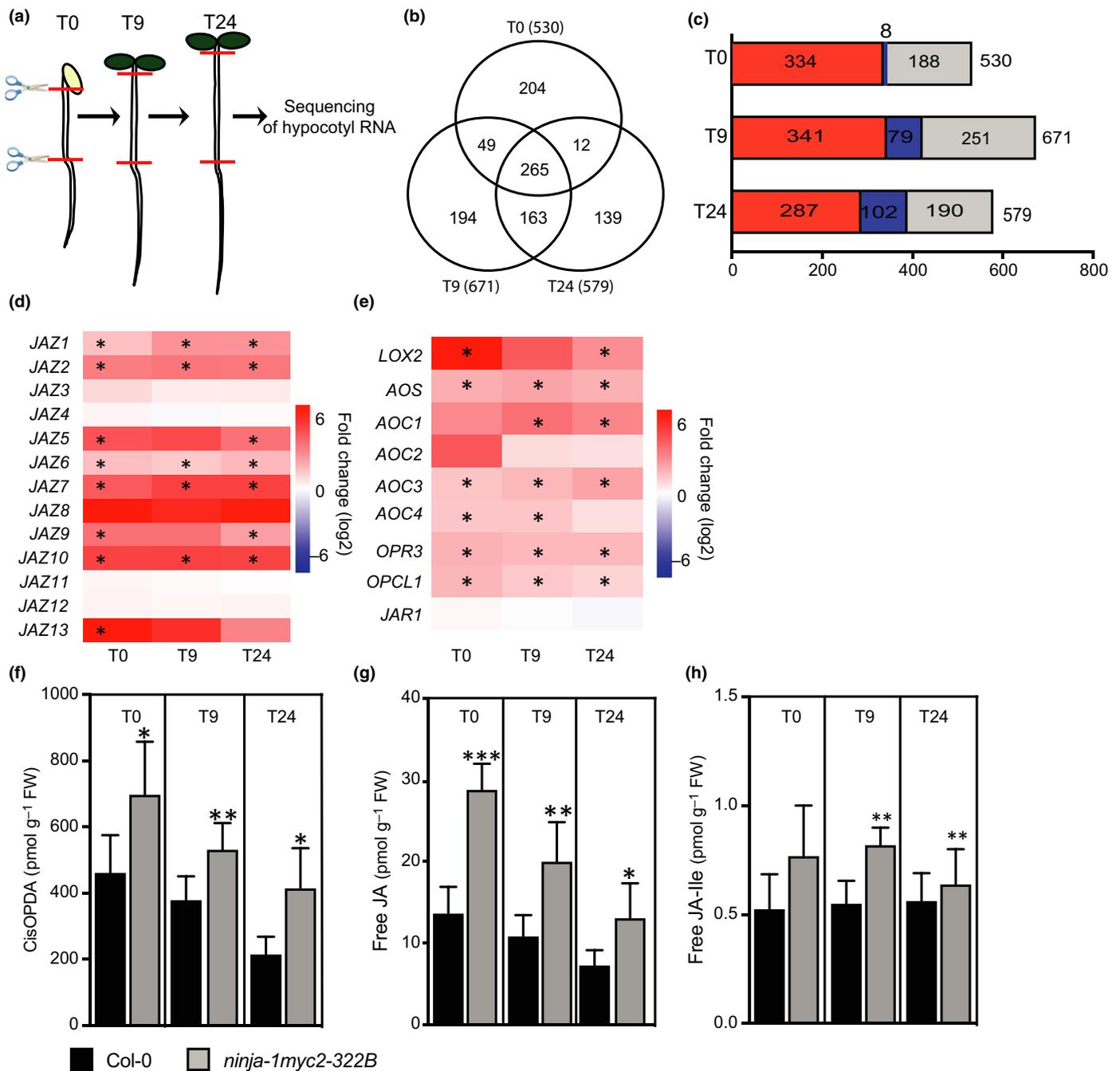
involved in JA biosynthesis, such as *LIPOXYGENASE 2* (*LOX2*), *ALLENE OXIDE SYNTHASE* (*AOS*), *ALLENE OXIDE CYCLASE1* (*AOC1*), *AOC3*, *AOC4*, *OXOPHYTODIENOATE-REDUCTASE3* (*OPR3*) and *OPC-8:0 COA LIGASE1* (*OPCL1*) were upregulated in the double mutant *ninja-1myc2-322B* (Fig. 4e). The biological relevance of this upregulation of gene expression was confirmed by findings that levels of the JA precursor *cis*-12-oxo-phytodienoic acid (*cis*-OPDA), JA and JA-Ile were higher in the double mutant than in wild-type controls at all time points, except that JA-Ile contents did not significantly differ at T0 (Fig. 4f–h). These data highlight a feedforward loop that amplifies the response to JA signaling by enhancing JA biosynthesis.

Fig. 4 RNA-Seq revealed several differentially expressed genes (DEGs) between the *ninja-1myc2-322B* double mutant and wild-type Arabidopsis seedlings. (a) Schematic representation of the RNA-Seq experiment. Total RNA was extracted from hypocotyls of *ninja-1myc2-322B* double mutant and wild-type seedlings grown in the dark until their hypocotyls were 6–7 mm long (T0), and after their transfer to the light for 9 h (T9) or 24 h (T24). (b) Venn diagram summarizing the DEGs between *ninja-1myc2-322B* double mutant and wild-type seedlings. (c) Enrichment of G-box (CACGTG, CACATG) or G-box-like (AACGTG, CATGTG CACGCG or CACGAG) motifs in the DEGs. Colors indicate upregulated genes (red) or downregulated genes (blue) containing at least one of the motifs. The gray color indicates the remaining DEGs, containing none of the mentioned motifs. (d) Heatmap of expression of the 13 *JAZ* genes. The map is based on fold-differences ($\log_2$) in transcript abundance (based on RNA-Seq data) in *ninja-1myc2-322B* double mutant samples relative to the abundance in wild-type samples. Colors indicate upregulated genes (red) and downregulated genes (blue) in *ninja-1myc2-322B* double mutant relative to expression levels in wild-type seedlings. Values marked with asterisks are statistically significant. (e) Heatmap of expression selected jasmonate (JA) biosynthesis genes. The map is based on fold-differences ($\log_2$) in transcript abundance (based on RNA-Seq data) in *ninja-1myc2-322B* double mutant samples relative to the abundance in wild-type samples. Colors indicate upregulated genes (red) and downregulated genes (blue) in *ninja-1myc2-322B* relative to wild-type expression levels. Values marked with asterisks are statistically significant. (f–h) Endogenous JA contents. (f) *cis*-OPDA, (g) free JA and (h) JA-Ile contents of hypocotyls of *ninja-1myc2-322B* and wild-type seedlings grown in the dark until their hypocotyls were 6 mm long (T0) and after their transfer to the light for 9 h (T9) and 24 h (T24). Asterisks indicate statistically significant differences between the mutant lines and wild-type plants according to analysis of variance (*, $0.05 > P > 0.01$; **, $0.01 > P > 0.001$; ***, $P < 0.001$, respectively). Error bars indicate $\pm$ SD of six biological replicates.
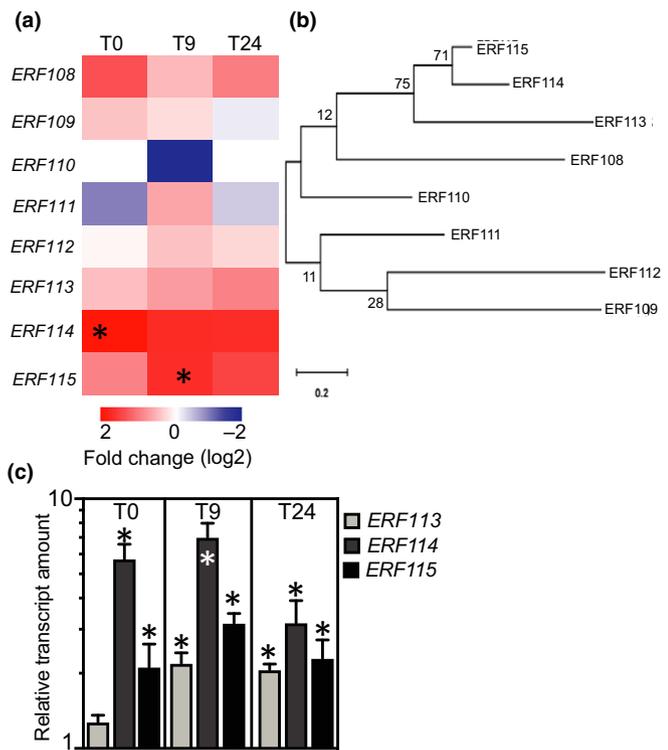
Fig. 5 *ERF113*, *ERF114* and *ERF115* are induced by jasmonate (JA) signaling. (a) Heatmap of expression of the subgroup X *ETHYLEN RESPONSE FACTOR (ERF)* family members. The map is based on fold-differences (log$_2$) in transcript abundance (based on RNA-Seq data) in *ninja-1myc2-322B* double mutant samples relative to the abundance in wild-type samples. Colors indicate upregulated genes (red) or downregulated genes (blue) in *ninja-1myc2-322B* relative to wild-type expression levels. Values marked with asterisks are statistically significant. (b) Phylogenetic tree of subgroup X of the AP2/ERF protein family derived from protein sequence alignment by the maximum likelihood method using MEGA X software (Kumar *et al.*, 2018). (c) Validation by qRT-PCR of mutation-induced shifts in *ERF113*, *ERF114* and *ERF115* expression profiles in the *ninja-1myc2-322B* double mutant (abundance of transcripts, in log$_{10}$ scale, at indicated time points relative to their abundance in wild-type seedlings, which was arbitrarily set to 1). Error bars indicate ± SE obtained from three independent technical replicates. Asterisks mark significance differences between the genotypes according to a *t*-test ($P < 0.001$, $n = 3$). The experiment was repeated twice with independent biological replicates and gave similar results.

cell replenishment (Heyman *et al.*, 2013, 2016; Zhou *et al.*, 2019) prompted us to address its function during ARI. First, to overcome potential functional redundancy with other members of the family, we analyzed the *pERF115:ERF115:SRDX* line, which expresses a dominant negative variant of ERF115 (because the *ERF115* coding sequence fused to the ethylene-responsive element binding factor-associated amphiphilic repression (EAR) domain is driven by the *ERF115* promoter to ensure repression in the native expression domain (Heyman *et al.*, 2013). The *pERF115:ERF115:SRDX* line produced significantly more ARs than wild-type controls but was very similar to the *rap2.6l-1erf114Cerf115* triple mutant (Fig. 6a,b). Although we cannot exclude a potential contribution of other *ERF* genes, these findings suggest that *ERF113*, *ERF114* and *ERF115* are the main

transcription factors involved in ARI. Interestingly, the overexpressing line *35S:ERF115* developed extremely few ARs (Fig. 6b) but had only slightly lower LR density than wild-type plants (Figs 6c, S4c,d). Thus, it phenocopied the *ninja-1myc2-322B* double mutant and confirmed that *ERF115* is an ARI repressor. We also characterized *ERF115*'s expression pattern during early ARI events using lines harboring the transcriptional fusion *pERF115:GUS* (Heyman *et al.*, 2013). At T0, GUS staining was mainly detected in vascular tissues of the hypocotyl, and to a lesser extent in the root (Fig. 6d). Exposing the seedlings to light for 24 h dramatically decreased the GUS signal (Fig. 6d), suggesting that the *ERF115* gene is expressed in vascular tissue and its expression is negatively regulated by light, which we confirmed by qRT-PCR (Fig. 6e).

As JA acts downstream of auxin signaling in ARI inhibition (Gutierrez *et al.*, 2012; Lakehal *et al.*, 2019a), we hypothesized that the *35S:ERF115* line could be insensitive to exogenously applied auxin. To test this hypothesis, we treated *35S:ERF115*-expressing and wild-type pre-etiolated seedlings with the synthetic auxin naphthaleneacetic acid (NAA), and found that 1 µM NAA significantly enhanced AR development in the wild-type seedlings, but did not affect the *35S:ERF115*-expressing seedlings (Fig. 6i–k). These data suggest that auxin cannot bypass the inhibitory effect of *ERF115* during ARI. Notably, the PR and LRs of the *35S:ERF115*-expressing seedlings were as sensitive as the wild-type roots to NAA (Fig. 6i,j). These data suggest that *ERF115* specifically activates and/or cooperates with other negative regulator(s) of ARI downstream of auxin signaling.

ERF115-mediated ARI repression requires CKs

Cytokinins, in balance with auxin, are known to promote shoot and callus formation but inhibit root growth and AR formation (Lakehal & Bellini, 2018; Ikeuchi *et al.*, 2019), raising the possibility that modulation of the CK machinery by *ERF115* is involved in this multifunctionality. We confirmed the negative role of CKs in control of ARI as exogenously applied 6-benzyladenine (6-BA) inhibited the process in a dose-dependent manner (Fig. 7a). We then analyzed the CK-deficient triple loss-of-function mutant *ipt3ipt5ipt7* that lacks three important ATP/ADP ISOPENTENYLTRANSFERASES catalyzing a rate-limiting step in *de novo* CK biosynthesis (Miyawaki *et al.*, 2006), and a line overexpressing *CYOKININ OXIDASE1* (*35S:CKX1*), which is also deficient in CKs due to their enhanced degradation (Werner *et al.*, 2003). Notably, both the triple loss-of-function mutant *ipt3ipt5ipt7* and the *35S:CKX1*-expressing line produced significantly more ARs than wild-type controls (Fig. 7b,c). Similarly, the *arr1-3arr11-2* double mutant and *arr1-3arr11-2arr12-1* triple mutant, which lack the key type-B transcription factors ARR1, ARR11 and ARR12 involved in CK signaling, produced significantly more ARs than wild-type plants (Fig. 7d). These data genetically confirmed that CKs are repressors of ARI.

To test the hypothesis that *ERF115* inhibits ARI through CKs, we quantified relative amounts of transcripts of two CK-responsive genes, *ARR5* and *ARR7*, in etiolated hypocotyls of the overexpressing line *35S:ERF115* and wild-type controls at T0 and
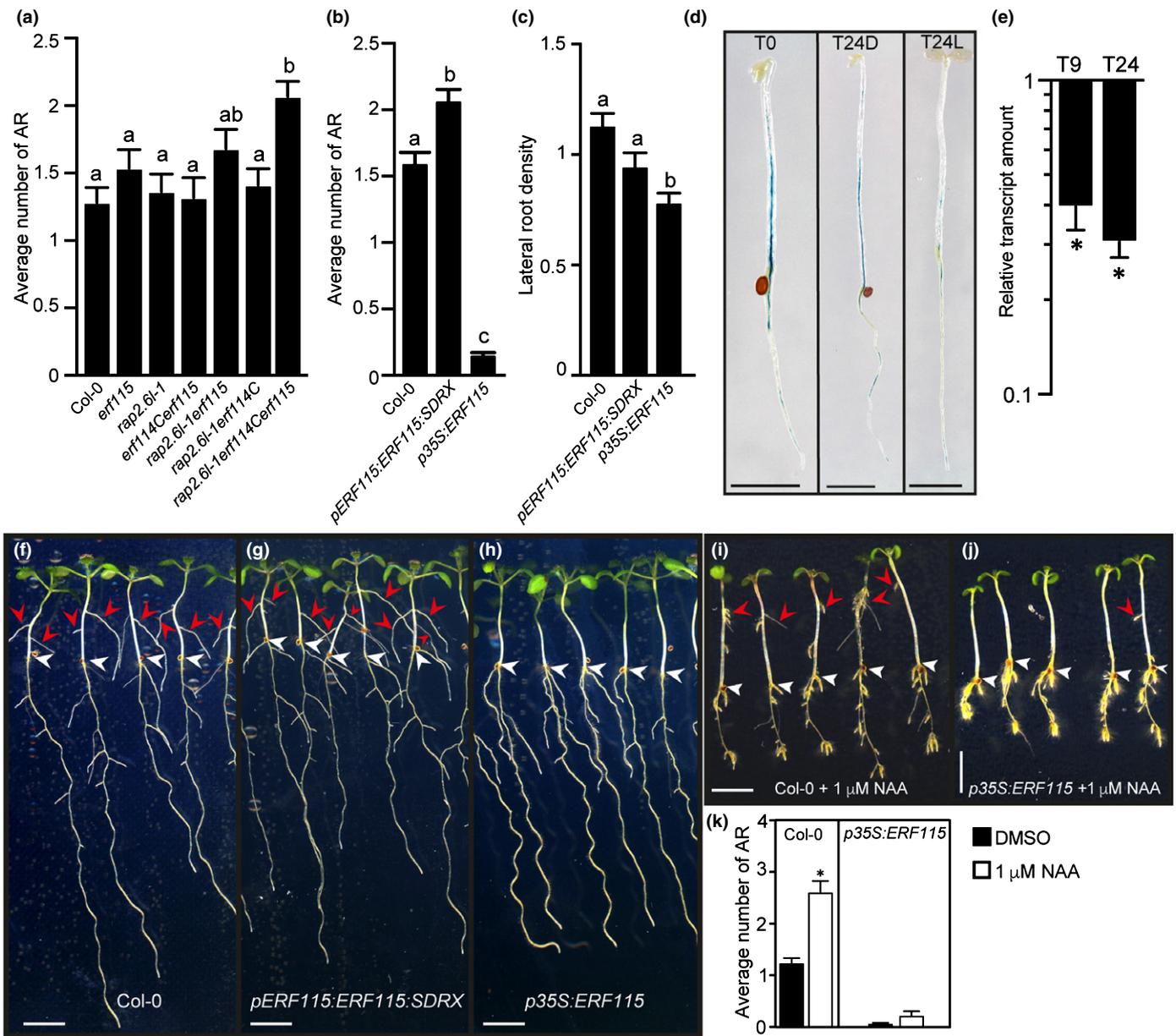
Fig. 6 The *ERF115* gene is an inhibitor of adventitious root initiation in Arabidopsis. (a) Average numbers of adventitious root (AR) produced by *erf* mutants and wild-type seedlings. One-way analysis of variance (ANOVA) combined with Tukey's multiple comparison post-test indicated that only the triple mutant *rap2-6Ierf114Cerf115* significantly differed in this respect from wild-type (Col-0) plants (denoted by letters). Error bars indicate ± SEM ($n \geq 40$, $P < 0.001$). (b) Average numbers of ARs produced by *35S:ERF115* and *pERF115:ERF115:SRDX* lines relative to numbers produced by wild-type plants. Data from two independent biological replicates, each of at least 40 seedlings, were pooled and averaged. A nonparametric Kruskal–Wallis test followed by Dunn's multiple comparison test indicated that numbers of ARs produced by the transgenic and wild-type plants significantly differed (denoted by letters). Error bars indicate ± SEM ($n \geq 40$, $P < 0.02$). (c) Lateral root (LR) density of *35S:ERF115* and *pERF115:ERF115:SRDX* lines and wild-type plants in AR phenotyping conditions. *35S:ERF115* mutants had significantly lower LR density than wild-type plants according to one-way ANOVA followed by Tukey's multiple comparison test (denoted by letters). (d) Spatiotemporal activity pattern of the *ERF115* promoter, as shown by seedlings expressing the *pERF115:GUS* construct grown in the dark until their hypocotyls were 6–7 mm long (T0), and 24 h (T24L) after either transfer to the light or further growth in the dark (T24D). Bars, 6 mm. (e) Validation by qRT-PCR of *ERF115* expression patterns in wild-type plants. Presented gene expression values are relative (in $\log_{10}$ scale) to the expression at T0, for which the value was arbitrarily set to 1. Error bars indicate ± SE obtained from three independent technical replicates. A *t*-test indicated that values indicated by an asterisks indicate values that significantly differ from the T0 values ($P < 0.001$, $n = 3$). The experiment was repeated twice with independent biological replicates and gave similar results. (f–h) Representative photos of (f) wild type, (g) *pERF115:ERF115:SRDX*, and (h) *35S:ERF115* seedlings. (i, j) Representative photographs of wild-type and *35S:ERF115* seedlings grown in the dark until their hypocotyls were 6–7 mm long, then transferred to fresh medium containing either mock solution or 1 μM naphthaleneacetic acid (NAA) for seven more days under long-day conditions to induce ARs. Arrowheads indicate hypocotyl-root junctions (white) or ARs (red). Bars, 6 mm. (k) Average numbers of ARs produced by wild-type and *35S:ERF115* plants in response to NAA. Wild-type seedlings produced significantly more ARs after NAA treatment than after mock-treatment according to a Mann–Whitney test, indicated by an asterisk ($n \geq 40$, $P < 0.0001$), but NAA treatment had no significant effect on AR production by *35S:ERF115* plants. Error bars indicate ± SEM.
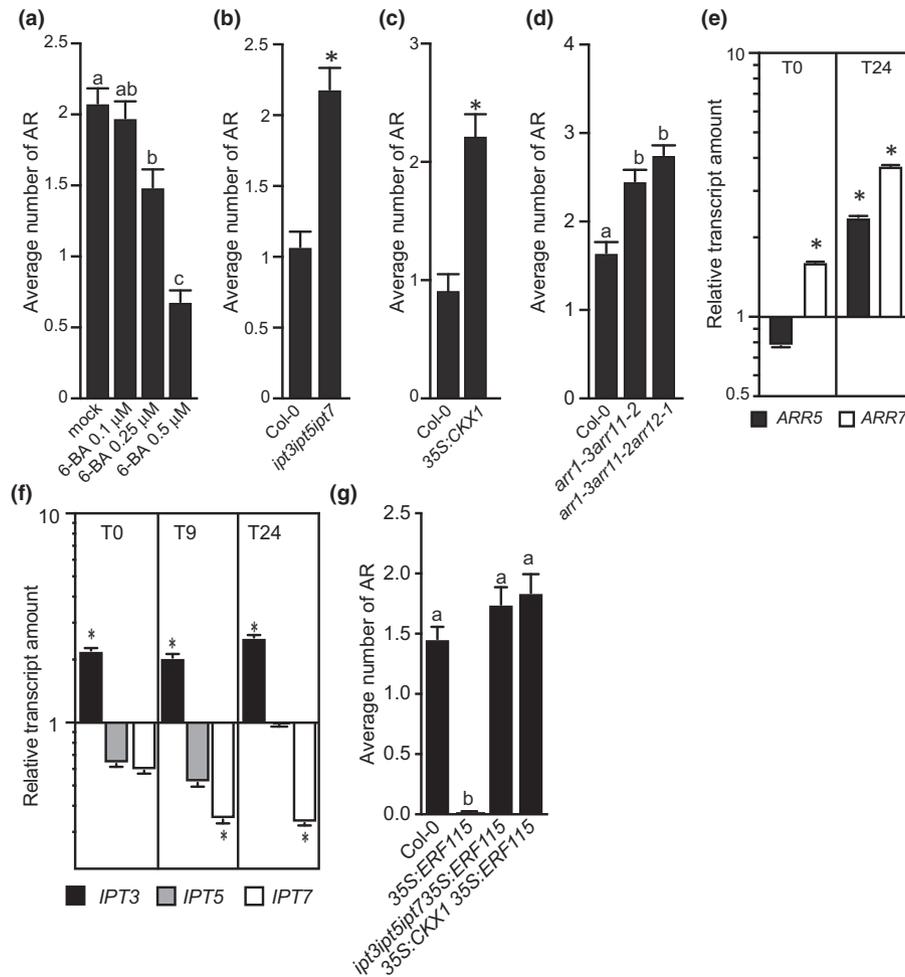
Fig. 7 Cytokinins inhibit adventitious root initiation downstream of *ERF115*. (a) Average numbers of adventitious roots (ARs) produced by wild-type (Col-0) seedlings, which were grown in the dark until their hypocotyls were 6–7 mm long, then transferred to fresh medium containing either mock solution or solutions with indicated concentrations of 6-benzylaminopurine (6-BA). The seedlings were kept for seven more days under long-day conditions to induce ARs. Seedlings treated with 0.25 or 0.5 µM 6-BA significantly differed from the mock-treated controls, according to a nonparametric Kruskal–Wallis test followed by Dunn's multiple comparison test (denoted by letters). Error bars indicate $\pm$ SEM ($n \geq 40$, $P < 0.004$). (b–d) Average numbers of ARs produced by wild-type plants and: (b) *ipt3ipt5ipt7* triple mutants defective in cytokinin (CK) biosynthesis, (c) *35S:CKX1 CYTOKININ OXIDASE1*-overexpressing plants, which have reduced CK contents due to increased rates of degradation, and (d) CK signaling mutants. (e) Relative amounts of *ARR5* and *ARR7* transcripts quantified by qRT-PCR. Total RNA was extracted from hypocotyls of *35S:ERF115* and the wild-type seedlings grown in AR-inducing conditions, as outlined earlier, at T0 (at the end of the dark incubation) and T24 (24 h later). The gene expression values are relative to wild-type values, which were arbitrarily set to 1. The y-axis scale is a $\log_{10}$ scale. Error bars indicate $\pm$ SEM obtained from three technical replicates. Asterisks indicate values that significantly differ from wild-type values according to a *t*-test ($P < 0.001$, $n = 3$). The experiment was repeated once with an independent biological replicate and gave similar results. (f) Relative amounts of *IPT3*, *IPT5* and *IPT7* transcripts quantified by qRT-PCR. Total RNA was extracted from hypocotyls of *35S:ERF115* and the wild-type seedlings grown in AR-inducing conditions, as outlined earlier, at T0 (at the end of the dark incubation), T9 and T24 (9 and 24 h later, respectively). The gene expression values are relative to wild-type values, which were arbitrarily set to 1. The y-axis scale is a $\log_{10}$ scale. Error bars indicate $\pm$ SEM obtained from three technical replicates. Asterisks indicate values that significantly differ from wild-type values according to a *t*-test ($P < 0.001$, $n = 3$). The experiment was repeated once with an independent biological replicate and gave similar results. (g) Average numbers of ARs produced by *35S:ERF115* plants, *35S:ERF115* plants overexpressing *CKX1* from a *35S:CKX1* construct and the *ipt3,5,7* triple mutant overexpressing *ERF115* from a *35S:ERF115* construct. Numbers produced by the multiple mutants significantly differed from numbers produced by *35S:ERF115* plants according to a nonparametric Kruskal–Wallis test followed by Dunn's multiple comparison test (denoted by letters). Error bars indicate $\pm$ SEM ($n \geq 40$, $P < 0.0001$).

T24. Interestingly, at T0 *ARR7* was upregulated, and at T24 both *ARR5* and *ARR7* were upregulated in the *35S:ERF115* line (Fig. 7e). These findings suggest that CK responses are enhanced in hypocotyls of *35S:ERF115* plants, and to explore possible causes we quantified the content of the active CK bases isopentyladenine (iP), *trans*-Zeatin (*tZ*) and *cis*-Zeatin (*cZ*) at T0, T9 and

T24. At T0, contents of iP, tZ and cZ in *35S:ERF115* and wild-type plants did not significantly differ (Fig. 8a). However, at T9, *35S:ERF115* plants had significantly higher iP, *tZ* and *cZ* contents, and at T24 significantly higher iP and *cZ* contents than wild-type controls (Fig. 8a). The accumulation of CK active bases could be due to an increase of *de novo* biosynthesis and/or to a
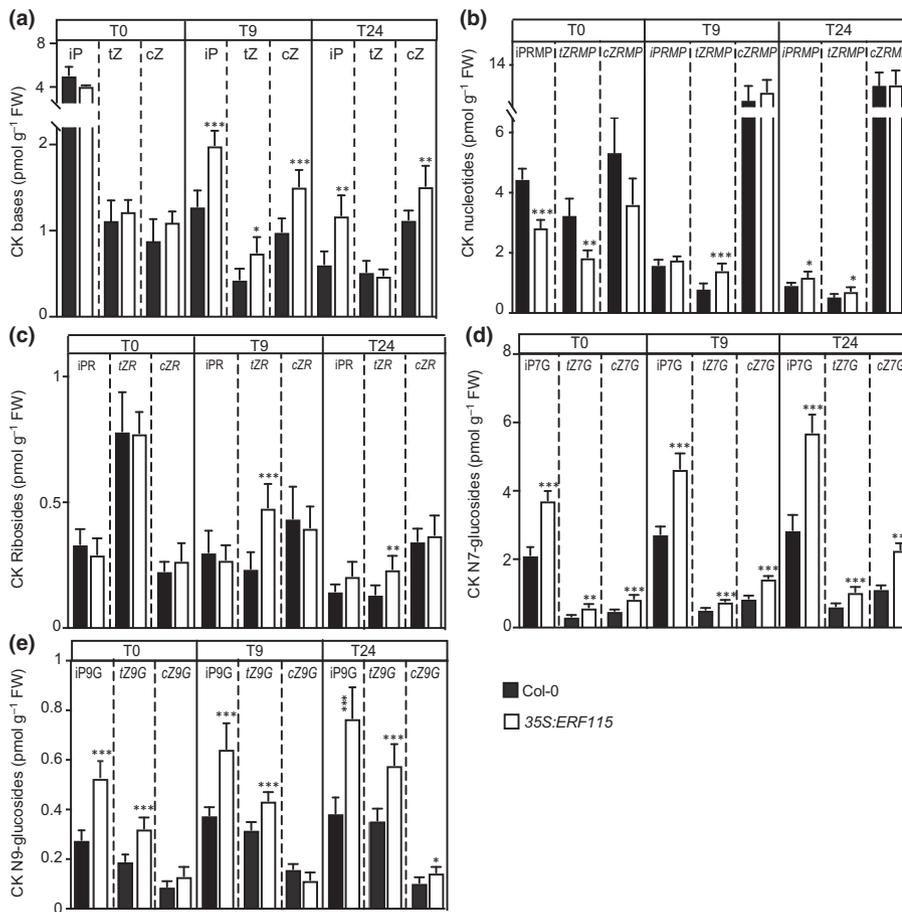
Fig. 8 *ERF115* controls *de novo* cytokinin (CK) biosynthesis at early stages of adventitious root initiation in Arabidopsis. (a–e) Endogenous CK contents. (a) CK active bases, (b) CK nucleotides, (c) CK ribosides, (d) CK *N7*-glucosides and (e) CK *N9*-glucosides. The CKs were quantified in the hypocotyls of *35S:ERF115* and the wild-type seedlings grown in the dark until they were 6 mm long (T0) and after their transfer to the light for 9 h (T9) or 24 h (T24). Asterisks indicate statistically significant differences between *35S:ERF115* and wild-type plants according to analysis of variance (*, **, and *** indicate *P*-values of 0.05 > *P* > 0.01, 0.01 > *P* > 0.001, and *P* < 0.001, respectively). Error bars indicate ± SD of six biological replicates.

reduced degradation or conjugation. To investigate these possibilities, we quantified the CK nucleotides (iPRMP, *t*ZRMP, *c*ZRMP) (Fig. 8b) and the CK ribosides (iPR, *t*ZR, *c*ZR) (Fig. 8c), which are the main CK precursors. We also quantified the CK *N*-glucosides (iP7G, *t*Z7G, *c*Z7G, iP9G, *t*Z9G, *c*Z9G) (Fig. 7d,e), which are regarded as the irreversible CK conjugates (Kieber & Schaller, 2014). At T0, *35S:ERF115* plants had significantly less iPRMP and *t*ZRMP compared to the wild type but at T9 *35S:ERF115* plants had significantly more *t*ZRMP and *t*ZR, and at T24, they had significantly more iPRMP, *t*ZRMP and *t*ZR compared to the wild type (Fig. 8b,c). Interestingly, *35S: ERF115* plants had also significantly more CK *N*-glucosides at all time point tested, except *c*Z9G at T0 and T9 (Fig. 8d,e). These data indicate that ERF115 promotes the accumulation of CK active bases by activating the biosynthesis pathways. The accumulation of the CK N-glucosides serves as a compensatory mechanism in order to maintain an optimum CK pool. Notably, The CK signaling and response are known to be tightly regulated by negative feedback loops through the induction of the CK conjugation pathways and/or the up-regulation of the expression of the *type-A ARRs* genes, which are negative regulators (Kieber & Schaller, 2014).

To get more evidence, we quantified the relative transcript amounts of key genes involved in CK biosynthesis (*IPT3*, *IPT5* and *IPT7*) in the *35S:ERF115* line and the wild type. Interestingly, *IPT3*, which encodes for an enzyme catalyzing the rate-

limiting step in CK biosynthesis (Miyawaki *et al.*, 2004, 2006), was consistently upregulated in the *35S:ERF115* compared to the wild type during the early stages of ARI (T0, T9 and T24), whereas its closely-related paralog *IPT5* (Miyawaki *et al.*, 2004, 2006) had a similar expression level in both genotypes (Fig. 7f). *IPT7*, another closely-related paralog of *IPT3* (Miyawaki *et al.*, 2004, 2006), was downregulated in *35S:ERF115* compared to the wild type (Fig. 7f), suggesting the presence of a potential transcriptional compensatory mechanism within the *IPT* gene family in order to keep balanced CK pools during ARI. These data suggest that *ERF115* positively controls the *de novo* CK biosynthesis by inducing the expression of *IPT3*. To get a genetic evidence, we generated a *35S:ERF115ipt3ipt5ipt7* multiple mutant and a line overexpressing both *35S:ERF115* and *35S:CKX1* to deplete the CK pool in a *35S:ERF115* background, and confirmed that this was sufficient to restore ARI to wild-type levels in the *35S: ERF115* line (Fig. 7g). These data confirm further that *ERF115* inhibition of ARI is mediated by CKs. Interestingly, our transcriptomic data showed that several *LONELY GUY* (*LOG*) genes, which control a rate-limiting step in CK biosynthesis (Kuroha *et al.*, 2009), were slightly upregulated, while several *CKX* genes were slightly downregulated, in the *ninja-1myc2-322B* double mutant (Fig. S5a,b). Often developmental programs, including ARI, are tightly controlled by complex feedback and feedforward loops (Gutierrez *et al.*, 2009; Lakehal *et al.*, 2019b). To investigate a possible perturbance of JA responses in the CK deficient

mutants, we quantified relative transcript amounts of *OPR3* a key gene involved in the JA biosynthesis, of *GH3.11/JAR1* which encodes the enzyme conjugating JA with isoleucine to produce the active form, and of the *MYC2* gene encoding the master transcriptional regulator as well as the expression of three *bona fide* JA-responsive genes (*JAZ3*, *JAZ5*, *JAZ10*) in the *ipt3ipt5ipt7* triple mutant and the *35S:CKX1*-expressing line. The expression levels of the genes tested were not changed in the *ipt3ipt5ipt7* triple mutant or the *35S:CKX1*-expressing line compared to the wild type at early stages of ARI, except of *JAZ5* and *JAZ10* which were slightly up regulated in *35S:CKX1* at T24 (Fig. S6a,b). These data suggest that JA signalling and biosynthesis are not perturbed in the *ipt3ipt5ipt7* triple mutant or the *35S:CKX1* expressing line.

Altogether, our results strongly suggest that JA inhibits ARI by modulating CK homeostasis through the action of *ERF115*.

Discussion

We have previously shown that auxin controls ARI in Arabidopsis hypocotyls by modulating JA homeostasis (Gutierrez *et al.*, 2009, 2012; Lakehal *et al.*, 2019a), but the JA signaling mechanism involved was not clear. Here, we provide detailed genetic and mechanistic insights into the JA signaling involved in ARI. Notably, *ninja-1* and *ninja-2* loss-of-function mutants produce ARs, albeit fewer than wild-type controls, and several lines of evidence indicate that this is possibly due to NINJA-independent repression of MYC-dependent machinery by a subset of JAZ proteins. For example, JAZ5, JAZ6, JAZ7 and JAZ8 can directly recruit TPL through their EAR motifs independently of NINJA (Kagale *et al.*, 2010; Causier *et al.*, 2012; Shyu *et al.*, 2012), while JAZ1, JAZ3 and JAZ9 can directly recruit HISTONE DEACETYLASE6 (HDA6) (Zhu *et al.*, 2011), which participates in repression of various JA-induced genes' expression (Zhu *et al.*, 2011). In addition, yeast two-hybrid experiments have shown that JAZ7, JAZ8 and JAZ13 do not interact with NINJA (Pauwels *et al.*, 2010; Shyu *et al.*, 2012; Thireault *et al.*, 2015), and the Jasmonate-associated (Jas) domain of JAZ directly binds to the region containing the JID and TAD of MYC2, MYC3 or MYC4 (Zhang *et al.*, 2015). Moreover, MED25 (one of 29 subunits of the MEDIATOR complex) interacts with MYC proteins and recruits the RNA polymerase II-dependent transcriptional machinery at MYC-target genes (Chen *et al.*, 2012; An *et al.*, 2017). MED25 directly interacts with the TAD of MYCs, raising the possibly that it competes with JAZ proteins for access to the TAD (Zhang *et al.*, 2015). All these findings suggest that some JAZ proteins might block transcriptional activities of MYC transcription factors involved in ARI in a NINJA-independent manner. Further research is needed to decipher the JAZ-dependent JA perception machinery involved in ARI. For this, combining mutants with potentially complementary functionalities, and/or potentially informative expression patterns, may be more illuminating than generating higher-order multiple mutants based on phylogenetic relationships.

Our results indicate that MYC-mediated JA signaling inhibits ARI in both NINJA-dependent and NINJA-independent manners. Both pathways act synergistically in control of the JA response, as indicated by the much lower numbers of ARs produced by *ninjamyc2-322B* double mutants than the parental lines (*ninja* and *myc2-322B*) and wild-type controls. Moreover, the *ninja1myc2-322B* double mutant exhibited a significant accumulation of JA and JA-Ile, which is due to an enhanced *de novo* biosynthesis as indicated by the up-regulation of the key genes in JA biosynthesis (*LOX2*, *AOS*, *AOC1*, *AOC3*, *AOC4*, *OPR3* and *OPCL1*) as well as metabolite quantifications (*cis*-OPDA). The accumulation of JA and JA-Ile in this mutant likely triggers the degradation of JAZ repressors, and thereby releases MYC2, MYC3 and MYC4 from the remaining NINJA-independent JAZ-mediated repression. It has also been demonstrated that JA plays a major role in stabilizing MYC2, MYC3 and MYC4 (Chico *et al.*, 2014). Hence, JA signaling seems to amplify further its response in a feedforward loop. Therefore, the strong phenotype of the *ninjamyc2-322B* double mutant may be due to an (almost) complete de-repression of not only MYC2, MYC3 and MYC4, but also of other NINJA-bound transcription factors (if any). Interestingly, this de-repression results in constitutively enhanced JA signaling. Accordingly, our transcriptomic analysis revealed that most of the JAZ genes, which are JA response marker genes (Chini *et al.*, 2007), were highly and constitutively upregulated in *ninja-1myc2-322B* plants throughout the covered developmental stages. Our results are consistent with a previous report suggesting that MYC2 controls root expansion in NINJA-dependent and NINJA-independent manners (Gasperini *et al.*, 2015).

For many years JA was regarded as a solely stress-related plant hormone, but more recently JA signaling has been implicated in several organogenesis and regenerative processes (Asahina *et al.*, 2011; Gutierrez *et al.*, 2012; Zhang *et al.*, 2019; Zhou *et al.*, 2019; Lakehal *et al.*, 2019a), and attempts to identify its downstream targets have begun. Although its role in adventitious rooting seems to be species- and context-dependent (Lakehal & Bellini, 2018), our results indicate that the *ERF115* gene is likely one of the targets acting downstream of JA in this process. This conclusion is strongly supported by the recent finding that MYC2 induces expression of *ERF115* by directly binding its promoter (Zhou *et al.*, 2019). The *ERF115* acts redundantly with its closely-related paralogs *ERF113* and *ERF114*, which have also been implicated in several organogenesis and regenerative processes (Heyman *et al.*, 2018). Here we provide evidence that *ERF115*-mediated ARI inhibition involves modulation of the CK machinery. Our data suggest that ERF115 promotes the *de novo* CK biosynthesis by inducing the expression of *IPT3* gene. Whether ERF115 directly binds to the *IPT3* promoter to directly control its expression remains to be addressed. Investigating this possibility will shed more light into the mechanistic basis on how JA-induced *ERF115* controls the CK pools. Physiological approaches have shown that CKs inhibit ARI in several plant species and model systems (Lakehal & Bellini, 2018). In this study, we genetically demonstrated that depleting CKs by either blocking their biosynthesis or enhancing their degradation restores the ARI wild-type phenotype in an *ERF115*-overexpressing line, confirming that *ERF115* represses ARI through CK

signaling. Consistent with the genetic evidence, we found that the expression of key genes in JA-Ile biosynthesis (*OPR3* and *GH3.11/JAR1*) and in JA signaling (*MYC2*, *JAZ3*, *JAZ5* and *JAZ10*) was not changed in CK deficient mutants, whereas the expression of genes involved in the CK biosynthesis or degradation was slightly upregulated or downregulated, respectively, in the *ninjamyc2-332B* double mutant indicating further that CK homeostasis is indeed under the control of JA signaling during the early stages of ARI. Interestingly, the *ERF115* promoter contains a CK-responsive motif, and a yeast one-hybrid screen has shown that ARR1 and ARR20 bind to the promoter of *ERF115* (Ikeuchi *et al.*, 2018). Although direct evidence is needed, these data suggest that cytokinin signaling may also control the abundance of *ERF115* transcripts. The role of this feedback loop in adventitious rooting, if any, awaits further investigation. Exploring further the exact mechanistic bases underlying the synergism between JA and CK signaling machineries will shed more light on ARI regulatory processes.

Acknowledgements

Author contributions

AL and CB conceived and designed the research; AL, AD, ZR, SA, SE, ON performed the research; AL, AD, ON analysed the data, AL, AD, CB wrote the manuscript; CB, HT, ON and MS acquired the funding.

ORCID

Sanaria Alallaq https://orcid.org/0000-0002-2961-6373
Catherine Bellini https://orcid.org/0000-0003-2985-6649
Asma Dob https://orcid.org/0000-0002-1013-1085
Sacha Escamez https://orcid.org/0000-0001-7049-6978
Abdellah Lakehal https://orcid.org/0000-0003-1943-6237
Ondřej Novák https://orcid.org/0000-0003-3452-0154
Zahra Rahneshan https://orcid.org/0000-0002-3995-6400
Miroslav Strnad https://orcid.org/0000-0002-2806-794X
Hannele Tuominen https://orcid.org/0000-0002-4949-3702

References

Acosta IF, Gasperini D, Chételat A, Stolz S, Santuari L, Farmer EE. 2013. Role of *NINJA* in root jasmonate signaling. *Proceedings of the National Academy of Sciences, USA* 110: 15473–15478.

An C, Li L, Zhai Q, You Y, Deng L, Wu F, Chen R, Jiang H, Wang H, Chen Q *et al.* 2017. Mediator subunit MED25 links the jasmonate receptor to transcriptionally active chromatin. *Proceedings of the National Academy of Sciences, USA* 114: E8930–E8939.

Andersen TG, Naseer S, Ursache R, Wybouw B, Smet W, De Rybel B, Vermeer JEM, Geldner N. 2018. Diffusible repression of cytokinin signalling produces endodermal symmetry and passage cells. *Nature* 555: 529–533.

Antoniadi I, Plačková L, Simonovik B, Doležal K, Turnbull C, Ljung K, Novák O. 2015. Cell-type-specific cytokinin distribution within the arabidopsis primary root apex. *Plant Cell* 27: 1955–1967.

Asahina M, Azuma K, Pitaksaringkarn W, Yamazaki T, Mitsuda N, Ohme-Takagi M, Yamaguchi S, Kamiya Y, Okada K, Nishimura T *et al.* 2011. Spatially selective hormonal control of *RAP2.6L* and *ANAC071* transcription factors involved in tissue reunion in Arabidopsis. *Proceedings of the National Academy of Sciences, USA* 108: 16128–16132.

Bellini C, Pacurar DI, Perrone I. 2014. Adventitious roots and lateral roots: similarities and differences. *Annual Review of Plant Biology* 65: 639–666.

Campos ML, Yoshida Y, Major IT, De Oliveira Ferreira D, Weraduwage SM, Froehlich JE, Johnson BF, Kramer DM, Jander G, Sharkey TD *et al.* 2016. Rewiring of jasmonate and phytochrome B signalling uncouples plant growth-defense tradeoffs. *Nature Communications* 7: 1–10.

Causier B, Ashworth M, Guo W, Davies B. 2012. The TOPLESS interactome: a framework for gene repression in Arabidopsis. *Plant Physiology* 158: 423–438.

Che P, Lall S, Nettleton D, Howell SH. 2006. Gene expression programs during shoot, root, and callus development in Arabidopsis tissue culture. *Plant Physiology* 141: 620–637.

Chen R, Jiang H, Li L, Zhai Q, Qi L, Zhou W, Liu X, Li H, Zheng W, Sun J *et al.* 2012. The arabidopsis Mediator subunit MED25 differentially regulates jasmonate and abscisic acid signaling through interacting with the MYC2 and ABI5 transcription factors. *Plant Cell* 24: 2898–2916.

Chico JM, Fernández-Barbero G, Chini A, Fernández-Calvo P, Díez-Díaz M, Solano R. 2014. Repression of jasmonate-dependent defenses by shade involves differential regulation of protein stability of MYC transcription factors and their JAZ repressors in Arabidopsis. *Plant Cell* 26: 1967–1980.

Chini A, Fonseca S, Fernández G, Adie B, Chico JM, Lorenzo O, García-Casado G, López-Vidriero I, Lozano FM, Ponce MR *et al.* 2007. The JAZ family of repressors is the missing link in jasmonate signalling. *Nature* 448: 666–671.

Chini A, Gimenez-Ibanez S, Goossens A, Solano R. 2016. Redundancy and specificity in jasmonate signalling. *Current Opinion in Plant Biology* 33: 147–156.

Clough SJ, Bent AF. 1998. Floral dip: a simplified method for Agrobacterium-mediated transformation of *Arabidopsis thaliana*. *The Plant Journal* 16: 735–743.

De Rybel B, Vassileva V, Parizot B, Demeulenaere M, Grunewald W, Audenaert D, Van Campenhout J, Overvoorde P, Jansen L, Vanneste S *et al.* 2010. A novel *Aux/IAA28* signaling cascade activates *GATA23*-dependent specification of lateral root founder cell identity. *Current Biology* 20: 1697–1706.

Floková K, Tarkowská D, Miersch O, Strnad M, Wasternack C, Novák O. 2014. UHPLC-MS/MS based target profiling of stress-induced phytohormones. *Phytochemistry* 105: 147–157.

Fonseca S, Chini A, Hamberg M, Adie B, Porzel A, Kramell R, Miersch O, Wasternack C, Solano R. 2009. (+)-7-iso-Jasmonoyl-L-isoleucine is the endogenous bioactive jasmonate. *Nature Chemical Biology* 5: 344–350.

Gasperini D, Chételat A, Acosta IF, Goossens J, Pauwels L, Goossens A, Dreos R, Alfonso E, Farmer EE. 2015. Multilayered organization of jasmonate signalling in the regulation of root growth. *PLoS Genetics* 11: 1–27.

Godoy M, Franco-Zorrilla JM, Pérez-Pérez J, Oliveros JC, Lorenzo Ó, Solano R. 2011. Improved protein-binding microarrays for the identification of DNA-binding specificities of transcription factors. *The Plant Journal* 66: 700–711.

Guo Q, Yoshida Y, Major IT, Wang K, Sugimoto K, Kapali G, Havko NE, Benning C, Howe GA. 2018. JAZ repressors of metabolic defense promote growth and reproductive fitness in *Arabidopsis*. *Proceedings of the National Academy of Sciences, USA* 115: E10768–E10777.

Gutierrez L, Bussell JD, Pacurar DI, Schwambach J, Pacurar M, Bellini C. 2009. Phenotypic plasticity of adventitious rooting in arabidopsis is controlled by complex regulation of *AUXIN RESPONSE FACTOR* transcripts and microRNA abundance. *Plant Cell* 21: 3119–3132.

Gutierrez L, Mongelard G, Floková K, Pǎcurar DI, Novák O, Staswick P, Kowalczyk M, Pǎcurar M, Demailly H, Geiss G *et al.* 2012. Auxin controls *arabidopsis* adventitious root initiation by regulating jasmonic acid homeostasis. *Plant Cell* 24: 2515–2527.

Heyman J, Canher B, Bisht A, Christiaens F, De Veylder L. 2018. Emerging role of the plant ERF transcription factors in coordinating wound defense responses and repair. *Journal of Cell Science* 131: jcs208215.

Heyman J, Cools T, Canher B, Shavialenka S, Traas J, Vercauteren I, Van Den Daele H, Persiau G, De Jaeger G, Sugimoto K *et al.* 2016. The heterodimeric transcription factor complex ERF115-PAT1 grants regeneration competence. *Nature Plants* 2: 1–7.

Heyman J, Cools T, Vandenbussche F, Heyndrickx KS, Van Leene J, Vercauteren I, Vanderauwera S, Vandepoele K, De Jaeger G, Van Der Straeten D *et al.* 2013. *ERF115* controls root quiescent center cell division and stem cell replenishment. *Science* 342: 860–863.

Ikeuchi M, Favero DS, Sakamoto Y, Iwase A, Coleman D, Rymen B, Sugimoto K. 2019. Molecular mechanisms of plant regeneration. *Annual Review of Plant Biology* 70: 377–406.

Ikeuchi M, Iwase A, Rymen B, Lambolez A, Kojima M, Takebayashi Y, Heyman J, Watanabe S, Seo M, De Veylder L *et al.* 2017. Wounding triggers callus formation via dynamic hormonal and transcriptional changes. *Plant Physiology* 175: 1158–1174.

Ikeuchi M, Shibata M, Rymen B, Iwase A, Bgman AM, Watt L, Coleman D, Favero DS, Takahashi T, Ahnert SE *et al.* 2018. A gene regulatory network for cellular reprogramming in plant regeneration. *Plant and Cell Physiology* 59: 765–777.

Kagale S, Links MG, Rozwadowski K. 2010. Genome-wide analysis of ethylene-responsive element binding factor-associated amphiphilic repression motif-containing transcriptional regulators in arabidopsis. *Plant Physiology* 152: 1109–1134.

Kieber JJ, Schaller GE. 2014. Cytokinins. *The Arabidopsis Book* 12: e0168.

Kong X, Tian H, Yu Q, Zhang F, Wang R, Gao S, Xu W, Liu J, Shani E, Fu C *et al.* 2018. Phb3 maintains root stem cell niche identity through ROS-responsive *AP2/ERF* transcription factors in arabidopsis. *Cell Reports* 22: 1350–1363.

Kumar S, Stecher G, Li M, Knyaz C, Tamura K. 2018. MEGA X: Molecular evolutionary genetics analysis across computing platforms. *Molecular Biology and Evolution* 35: 1547–1549.

Kuroha T, Tokunaga H, Kojima M, Ueda N, Ishida T, Nagawa S, Fukuda H, Sugimoto K, Sakakibara H. 2009. Functional analyses of LONELY GUY cytokinin-activating enzymes reveal the importance of the direct activation pathway in Arabidopsis. *Plant Cell* 21: 3152–3169.

Lakehal A, Bellini C. 2018. Control of adventitious root formation: insights into synergistic and antagonistic hormonal interactions. *Physiologia Plantarum* 165: 90–100.

Lakehal A, Chaabouni S, Cavel E, Le Hir R, Ranjan A, Raneshan Z, Novák O, Pǎcurar DI, Perrone I, Jobert F *et al.* 2019a. A molecular framework for the control of adventitious rooting by TIR1/AFB2-AUX/IAA-dependent auxin signaling in Arabidopsis. *Molecular Plant* 12: 1499–1514.

Lakehal A, Dob A, Novák O, Bellini C. 2019b. A *DAO1*-mediated circuit controls auxin and jasmonate crosstalk robustness during adventitious root initiation in arabidopsis. *International Journal of Molecular Sciences* 20: 4428.

Lakehal A, Ranjan A, Bellini C. 2020. Multiple roles of jasmonates in shaping rhizotaxis: emerging integrators. In: Champion A, Laplaze L (eds) *Jasmonate in plant biology. Methods in Molecular Biology.* New York, NY, USA: Humana, 3–22.

Langmead B, Salzberg SL. 2012. Fast gapped-read alignment with Bowtie 2. *Nature Methods* 9: 357–359.

Li B, Dewey CN. 2014. RSEM: accurate transcript quantification from RNA-seq data with or without a reference genome. *BMC Bioinformatics* 12: 41–74.

Mehrnia M, Balazadeh S, Zanor MI, Mueller-Roeber B. 2013. *EBE*, an *AP2/ERF* transcription factor highly expressed in proliferating cells, affects shoot architecture in Arabidopsis. *Plant Physiology* 162: 842–857.

Miyawaki K, Matsumoto-Kitano M, Kakimoto T. 2004. Expression of cytokinin biosynthetic isopentenyltransferase genes in Arabidopsis: tissue specificity and regulation by auxin, cytokinin, and nitrate. *The Plant Journal* 37: 128–138.

Miyawaki K, Tarkowski P, Matsumoto-Kitano M, Kato T, Sato S, Tarkowska D, Tabata S, Sandberg G, Kakimoto T. 2006. Roles of Arabidopsis ATP/ADP isopentenyltransferases and tRNA isopentenyltransferases in cytokinin biosynthesis. *Proceedings of the National Academy of Sciences, USA* 103: 16598–16603.

Nakano T, Suzuki K, Fujimura T, Shinshi H. 2006. Genome-wide analysis of the *ERF* gene family in arabidopsis and rice. *Plant Physiology* 140: 411–432.

Pauwels L, Barbero GF, Geerinck J, Tilleman S, Grunewald W, Pérez AC, Chico JM, Vanden Bossche R, Sewell J, Gil E *et al.* 2010. *NINJA* connects the co-repressor *TOPLESS* to jasmonate signalling. *Nature* 464: 788–791.

Rittenberg D, Foster GL. 1940. A new procedure for quantitative analysis by isotope dilution, with application to the determination of amino acids and fatty acids. *Journal of Biological Chemistry* 133: 737–744.

Schindelin J, Arganda-Carreras I, Frise E, Kaynig V, Longair M, Pietzsch T, Preibisch S, Rueden C, Saalfeld S, Schmid B *et al.* 2012. Fiji: an open-source platform for biological-image analysis. *Nature methods* 9: 676–682.

Sheard LB, Tan X, Mao H, Withers J, Ben-Nissan G, Hinds TR, Kobayashi Y, Hsu FF, Sharon M, Browse J *et al.* 2010. Jasmonate perception by inositol-phosphate-potentiated COI1-JAZ co-receptor. *Nature* 468: 400–407.

Shyu C, Figueroa P, DePew CL, Cooke TF, Sheard LB, Moreno JE, Katsir L, Zheng N, Browse J, Howe GA. 2012. JAZ8 lacks a canonical degron and has an ear motif that mediates transcriptional repression of jasmonate responses in Arabidopsis. *Plant Cell* 24: 536–550.

Smolen GA, Pawlowski L, Wilensky SE, Bender J. 2002. Dominant alleles of the basic helix-loop-helix transcription factor ATR2 activate stress-responsive genes in arabidopsis. *Genetics* 161: 1235–1246.

Sorin C, Bussell JD, Camus I, Ljung K, Kowalczyk M, Geiss G, McKhann H, Garcion C, Vaucheret H, Sandberg G *et al.* 2005. Auxin and light control of adventitious rooting in *Arabidopsis*. *Plant Cell* 17: 1343–1359.

Staswick PE, Sut W, Howell SH. 1992. Methyl jasmonate inhibition of root growth and induction of a leaf protein are decreased in an Arabidopsis thaliana mutant. *Proceedings of the National Academy of Sciences, USA* 89: 6837–6840.

Steffens B, Rasmussen A. 2016. The physiology of adventitious roots. *Plant Physiology* 170: 603–617.

Sukumar P, Maloney GS, Muday GK. 2013. Localized induction of the ATP-Binding Cassette B19 auxin transporter enhances adventitious root formation in arabidopsis. *Plant Physiology* 162: 1392–1405.

Svačinová J, Novák O, Plačková L, Lenobel R, Holík J, Strnad M, Doležal K. 2012. A new approach for cytokinin isolation from Arabidopsis tissues using miniaturized purification: pipette tip solid-phase extraction. *Plant Methods* 8: 1–14.

Tarazona S, García-Alcalde F, Dopazo J, Ferrer A, Conesa A. 2011. Differential expression in RNA-seq: a matter of depth. *Genome Research* 21: 2213–2223.

Thines B, Katsir L, Melotto M, Niu Y, Mandaokar A, Liu G, Nomura K, He SY, Howe GA, Browse J. 2007. JAZ repressor proteins are targets of the SCFCOI1 complex during jasmonate signalling. *Nature* 448: 661–665.

Thireault C, Shyu C, Yoshida Y, St. Aubin B, Campos ML, Howe GA. 2015. Repression of jasmonate signaling by a non-TIFY JAZ protein in Arabidopsis. *The Plant Journal* 82: 669–679.

Wang ZP, Xing HL, Dong L, Zhang HY, Han CY, Wang XC, Chen QJ. 2015. Egg cell-specific promoter-controlled CRISPR/Cas9 efficiently generates homozygous mutants for multiple target genes in Arabidopsis in a single generation. *Genome Biology* 16: 1–12.

Wasternack C, Hause B. 2013. Jasmonates: biosynthesis, perception, signal transduction and action in plant stress response, growth and development. An update to the 2007 review in Annals of Botany. *Annals of Botany* 111: 1021–1058.

Werner T, Motyka V, Laucou V, Smets R, Van Onckelen H, Schmülling T. 2003. Cytokinin-deficient transgenic arabidopsis plants show multiple developmental alterations indicating opposite functions of cytokinins in the regulation of shoot and root meristem activity. *Plant Cell* 15: 2532–2550.

Xie DX, Feys BF, James S, Nieto-Rostro M, Turner JG. 1998. COI1: an Arabidopsis gene required for jasmonate-regulated defense and fertility. *Science* 280: 1091–1094.

Xing H-L, Wang Z-P, Zhang H-Y, Han C-Y, Liu B, Wang X-C, Chen Q-J, Dong L. 2014. A CRISPR/Cas9 toolkit for multiplex genome editing in plants. *BMC Plant Biology* 14: 372.

Yan Y, Stolz S, Chételat A, Reymond P, Pagni M, Dubugnon L, Farmer EE. 2007. A downstream mediator in the growth repression limb of the jasmonate pathway. *Plant Cell* 19: 2470–2483.

Yang S, Poretska O, Sieberer T. 2018. *ALTERED MERISTEM PROGRAM1* restricts shoot meristem proliferation and regeneration by limiting HD-ZIP III-mediated expression of *RAP2.6l*. *Plant Physiology* 177: 1580–1594.

Zhang F, Yao J, Ke J, Zhang L, Lam VQ, Xin XF, Zhou XE, Chen J, Brunzelle J, Griffin PR *et al.* 2015. Structural basis of JAZ repression of MYC transcription factors in jasmonate signalling. *Nature* 525: 269–273.

Zhang G, Zhao F, Chen L, Pan Y, Sun L, Bao N, Zhang T, Cui CX, Qiu Z, Zhang Y *et al.* 2019. Jasmonate-mediated wound signalling promotes plant regeneration. *Nature Plants* 5: 491–497.

Zhou W, Lozano-Torres JL, Blilou I, Zhang X, Zhai Q, Smant G, Li C, Scheres B. 2019. A jasmonate signaling network activates root stem cells and promotes regeneration. *Cell* 177: 942–956.e14.

Zhu Z, An F, Feng Y, Li P, Xue L, Jiang Z, Kim J-m, To TK, Li W, Zhang X *et al.* 2011. Derepression of ethylene-stabilized transcription factors (*EIN3/EIL1*) mediates jasmonate and ethylene signaling synergy in Arabidopsis. *Proceedings of the National Academy of Sciences, USA* 108: 12539–12544.

Supporting Information

Additional Supporting Information may be found online in the Supporting Information section at the end of the article.

Fig. S1 Jasmonate signaling affects primary root (PR) length and lateral root (LR) number.

Fig. S2 Numbers of DEGs detected in RNA-Seq experiments.

Fig. S3 Illustration of the CRISPR-Cas9 strategy.

Fig. S4 Overexpressing *ERF115* affects the lateral root number.

Fig. S5 Heatmaps of expression of LOG genes and CKX genes.

Fig. S6 The expression of genes involved in JA biosynthesis or signaling is not affected in CK deficient mutants.

Table S1 Primers used for qRT-PCR, cloning and genotyping.

Table S2 List of differentially expressed genes (DEGs) between the wild type and the double mutant ninja–1myc2-322B.

Please note: Wiley Blackwell are not responsible for the content or functionality of any Supporting Information supplied by the authors. Any queries (other than missing material) should be directed to the *New Phytologist* Central Office.